

Maximum Likelihood Learning of Latent Dynamics Without Reconstruction

Samo Hromadka^{1,*} Kai Biegun² Lior Fox¹ James Heald¹ Maneesh Sahani¹

Abstract

We introduce a novel unsupervised learning method for time series data with latent dynamical structure: the recognition-parametrized Gaussian state space model (RP-GSSM). The RP-GSSM is a probabilistic model that learns Markovian Gaussian latents explaining statistical dependence between observations at different time steps, combining the intuition of contrastive methods with the flexible tools of probabilistic generative models. Unlike contrastive approaches, the RP-GSSM is a valid probabilistic model learned via maximum likelihood. Unlike generative approaches, the RP-GSSM has no need for an explicit network mapping from latents to observations, allowing it to focus model capacity on inference of latents. The model is both tractable and expressive: it admits exact inference thanks to its jointly Gaussian latent prior, while maintaining expressivity with an arbitrarily nonlinear neural network link between observations and latents. These qualities allow the RP-GSSM to learn task-relevant latents without ad-hoc regularization, auxiliary losses, or optimizer scheduling. We show how this approach outperforms alternatives on problems that include learning nonlinear stochastic dynamics from video, with or without background distractors. Our results position the RP-GSSM as a useful foundation model for a variety of downstream applications.

1 Introduction

Time series are ubiquitous in both machine and natural learning. In applications such as reinforcement learning (Zhang et al., 2021), robotics (Zhang et al., 2019), navigation (Çatal et al., 2021), or behavioral neuroscience (Friston et al., 2021), agents observe streams of data from which they must infer the state of their environment and, sometimes, predict future states. Observations are often high-dimensional, and agents should be able to infer relevant low-dimensional states in an unsupervised fashion; indeed, this ability is a hallmark of human behavior (Orbán et al., 2008). Time series observations are often driven by underlying latent dynamics, formalized by a *state space model* (SSM; Figure 1e). Most existing SSM learning methods are either *generative* or *contrastive*.

Generative methods parametrize a joint distribution between latents and observations and maximize the data likelihood (or a lower bound thereof). Crucially, the joint distribution is defined using an explicit likelihood that models how observations are generated from latents. Generative models in which learning and inference are tractable have limited expressivity; see Section 2.2. Learning more complex models requires approximation.

Deep neural networks have been integrated into state space modeling in recent years, most commonly using the variational autoencoder (VAE; Gregor et al., 2015; Johnson et al., 2016). VAEs are trained using approximate maximum likelihood estimation, enjoying convergence guarantees and principled uncertainty estimation. They work by learning a variational posterior parametrized by a recognition network (or “encoder”), which is trained concurrently with the generative network (or “decoder”).

¹Gatsby Unit, UCL

²AI Centre, UCL

*Correspondence to: s.hromadka@ucl.ac.uk

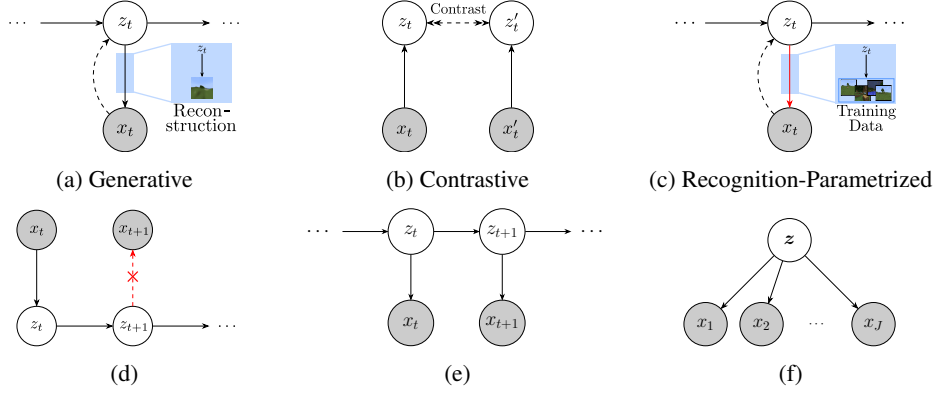


Figure 1: **(a)**: Generative methods learn by approximately reconstructing data; **(b)**: Contrastive methods learn by contrasting representations of data from distinct sequences; **(c)**: Recognition-parametrized methods learn by implicitly specifying a degenerate decoder that can only generate training data and enforcing conditional independence between observations given latents; **(d)**: In many applications, future latent variables are predicted, but not future observations; **(e)**: The SSM graphical model; **(f)**: Latent variable model with multiple observation factors.

Thus, a trained VAE can perform both recognition and generation. However, in many problem domains, such as decision making and control, agents require prediction of future latent states but *not* future observations (Figure 1d). In such applications, training a generative network is computationally wasteful and can be detrimental to learning. Indeed, VAE-based losses can be interpreted as regularized reconstruction objectives, which encourage latents to encode information about all aspects of the data, including irrelevant distractor features (Figure 1a). Another source of error is that generative models that are sufficiently flexible to model real-world data must resort to approximations in inference. These approximations in the variational posterior then bias decoder parameter estimates (Turner and Sahani, 2011), which in turn directs the encoder towards the wrong generative target (Cremer et al., 2018).

Contrastive methods, on the other hand, learn latent representations without modeling how observations are generated. Instead, they train a recognition network to contrast “positive” observations from “negative” ones (Figure 1b). Contrastive methods do not learn a full probabilistic state space model, obtaining neither latent dynamics nor posterior beliefs over latent variables—features that are crucial to optimal Bayesian decision making. Recent extensions suggest learning dynamics and uncertainty (Kirchhof et al., 2023; You et al., 2022), but even these do not restore a fully likelihood-based approach, instead depending on auxiliary losses and regularization.

In this work, we aim to improve state space recognition by combining the best of both worlds: utilizing the likelihood formalism of probabilistic models, but without an explicit generative “decoder” (Figure 1c). We do this in the framework of the recognition-parametrized model (RPM; Walker et al., 2023). Applied to an SSM, the RPM focuses on the intuition that observations at different times are conditionally independent given the true latents (Figure 1e), learning a probabilistic recognition model to infer latents that fit this description. As a result, the learned latents reflect temporally persistent features of the data while systematically ignoring distractors with unreliable statistics across time. We define an RPM with joint Gaussian latent prior that matches the SSM structure, derive the learning algorithm, and demonstrate its efficacy across a range of unsupervised time series datasets. The resulting RP-GSSM is, to the best of our knowledge, the first fully probabilistic method for modeling latent time series that does not learn an explicit generative model.

2 Background

2.1 Recognition-Parametrized Models

We first introduce the RPM in its general form, following Walker et al. (2023). Consider a latent-variable model where the observation $\mathbf{x} := (x_1, \dots, x_J)$ comprises multiple variables (i.e., $J > 1$) that are conditionally independent given the latents (Figure 1f):

$$x_i \perp\!\!\!\perp x_j \mid \mathbf{z} \quad \forall i \neq j.$$

The boldface \mathbf{z} may represent many latent variables with internal conditional independence structure, such as a Markov chain (Section 3). The graphical model in Figure 1f implies a joint distribution on latents \mathbf{z} and data \mathbf{x} :

$$p(\mathbf{x}, \mathbf{z}) = p(\mathbf{z}) \prod_{j=1}^J p(x_j | \mathbf{z}).$$

Equivalently, by Bayes' rule,

$$p(\mathbf{x}, \mathbf{z}) = p(\mathbf{z}) \prod_{j=1}^J \frac{p(\mathbf{z} | x_j) p(x_j)}{p(\mathbf{z})}.$$

Given a dataset $\mathbf{X} = (x_1^n, \dots, x_J^n)_{n=1}^N$, Walker et al. (2023) propose to model the true $p(\mathbf{x}, \mathbf{z})$ with a semi-parametric distribution $\tilde{p}_\theta^{\mathbf{X}}(\mathbf{x}, \mathbf{z})$ called the *RPM joint*, given by

$$\tilde{p}_\theta^{\mathbf{X}}(\mathbf{x}, \mathbf{z}) = p_\eta(\mathbf{z}) \prod_{j=1}^J \frac{f_{\phi_j}(\mathbf{z} | x_j) p_0(x_j)}{F_{\phi_j}(\mathbf{z})}, \quad (1)$$

where $\theta = (\eta, \{\phi_j\}_{j=1}^J)$ and

- $p_\eta(\mathbf{z})$ is a parametrization of the prior;
- $f_{\phi_j}(\mathbf{z} | x_j)$ are parametrized x_j -dependent distributions over \mathbf{z} called *recognition factors*;
- $p_0(x_j)$ is the empirical data distribution $p_0(x_j) = \frac{1}{N} \sum_{n=1}^N \delta(x_j = x_j^n)$;
- $F_{\phi_j}(\mathbf{z})$ ensures that the RPM joint is normalized:

$$F_{\phi_j}(\mathbf{z}) = \int f_{\phi_j}(\mathbf{z} | x_j) p_0(x_j) dx_j = \frac{1}{N} \sum_{n=1}^N f_{\phi_j}(\mathbf{z} | x_j^n). \quad (2)$$

The superscript \mathbf{X} in the RPM joint emphasizes that it is itself a function of the training data through its dependence on the empirical distributions $p_0(x_j)$.

Equation (1) defines a joint distribution over observed and latent variables that does not include a parametric component modeling a distribution on observations. Hence, the RPM circumvents learning an explicit generative model, allowing it to focus model capacity on learning good recognition factors. In fact, the generative distribution implied by the RPM joint in Equation (1) is

$$\tilde{p}_\theta^{\mathbf{X}}(\mathbf{x} | \mathbf{z}) \propto \prod_{j=1}^J f_{\phi_j}(\mathbf{z} | x_j) p_0(x_j),$$

so in a formal sense the RPM can only ever generate values of x_j that appear in the training set. However, as recognition is parametric, the RPM can nonetheless be used to construct posterior beliefs over latents given previously unseen observations.

Notably, the RPM joint is a normalized distribution and can be fit by maximum likelihood using the Expectation Maximization (EM) algorithm and related methods (Dempster et al., 1977). Walker et al. (2023) implement RPMs in a variety of settings and construct approximations when necessary. We apply some of their methods in Section 3.

2.2 State Space Models

A probabilistic SSM¹ is a latent variable model with Markovian latents $\mathbf{z} := (z_1, \dots, z_T)$, $z_t \in \mathbb{R}^{\mathcal{D}_z}$, and noisy, partially informative observations $\mathbf{x} := (x_1, \dots, x_T)$, $x_t \in \mathbb{R}^{\mathcal{D}_x}$.

The graphical model shown in Figure 1e provides the joint factorization over both \mathbf{x} and \mathbf{z} :

$$p(\mathbf{x}, \mathbf{z}) = p(z_1) \prod_{t=1}^{T-1} p(z_{t+1} | z_t) \prod_{t=1}^T p(x_t | z_t). \quad (3)$$

¹We use the term ‘‘SSM’’ to refer a generic probabilistic model with graphical structure as in Figure 1e, not the deterministic methods in recent literature on structured state space models, e.g. Mamba (Gu and Dao, 2024).

The standard approach to fitting an SSM to data is to parametrize the model with some parameters θ , define a *variational posterior* $q(\mathbf{z}) \approx p_\theta(\mathbf{z}|\mathbf{x})$, and maximize the *free energy*

$$\mathcal{F}(q, \theta) = \langle \log p_\theta(\mathbf{x}, \mathbf{z}) \rangle_{q(\mathbf{z})} + \mathcal{H}(q),$$

where $\langle \cdot \rangle_{q(\mathbf{z})}$ denotes expectation with respect to q and $\mathcal{H}(q) = -\langle \log q(\mathbf{z}) \rangle_{q(\mathbf{z})}$ is the entropy of q . The free energy is a lower bound to the data log-likelihood, $\log p_\theta(\mathbf{x})$, and can be maximized via the EM algorithm, consisting of alternating updates to q (“E-step”) and θ (“M-step”) (Dempster et al., 1977). Although the EM algorithm can be performed exactly for discrete latent variables (Baum and Petrie, 1966)—albeit with exponential computational complexity in latent dimensionality—in this work we focus on continuous latent variables. In this setting, there are few models for which EM can be performed exactly.

2.2.1 Linear-Gaussian SSM

In a *Gaussian SSM* (GSSM), the components of the prior distribution over the latents take the following jointly Gaussian form:

$$p(z_1) = \mathcal{N}(m_1, Q_1), \quad p(z_t|z_{t-1}) = \mathcal{N}(Az_{t-1} + b, Q).$$

When paired with linear-Gaussian emissions $p(x_t|z_t) = \mathcal{N}(Cz_t + d, R)$, the model is called a *linear-Gaussian SSM*. The E-step is solved exactly by Kalman smoothing (Kalman, 1960) and the M-step can be performed in closed form (Ghahramani and Hinton, 1996). In general, the parameters $(m_1, Q_1, A, b, Q, C, d, R)$ can vary over time, but we assume them to be time-invariant for notational simplicity. We call $p(z_1)$ the *initial distribution*, A the *transition matrix*, and b the *bias*. Although often chosen for tractability, the combination of linear dynamics and emission distributions is restrictive for many real-world applications. Therefore, in this work, we instead consider extensions to nonlinear-Gaussian emissions: $p(x_t|z_t) = \mathcal{N}(f(z_t), g(z_t))$.

2.2.2 Stability of Gaussian SSMs

We briefly review the theory of these models, inspired by Buesing et al. (2012). A GSSM is *stable* if $\rho(A) < 1$, where $\rho(\cdot)$ denotes the largest eigenvalue magnitude. A stable system has a well-defined *stationary distribution* $\lim_{t \rightarrow \infty} p(z_t)$ (Buesing et al., 2012). The following lemma shows that, in consequence of the non-identifiability of the GSSM parameters, no generality is lost by assuming that a latent process underlying a stable GSSM has zero transition bias and stationary distribution $\mathcal{N}(0, I)$.

Lemma 2.1 *Let the GSSM on observations $\mathbf{x} = (x_1 \dots, x_T)$ and latents $\mathbf{z} = (z_1, \dots, z_T)$, with parameters $\Theta = (m_1, Q_1, A, b, Q, f, g)$ be stable. Then there exists another stable GSSM with parameters $\tilde{\Theta} = (\tilde{m}_1, \tilde{Q}_1, \tilde{A}, \tilde{b}, \tilde{Q}, \tilde{f}, \tilde{g})$ such that*

$$p(\mathbf{x}|\Theta) = p(\mathbf{x}|\tilde{\Theta}),$$

the stationary distribution of the latent variables is $\mathcal{N}(0, I)$, and $\tilde{b} = 0$.

We provide a proof of Lemma 2.1 and an explicit form of $\tilde{\Theta}$ in Appendix A.

3 RP-GSSM

In this section we apply the RPM framework to the GSSM and develop the necessary approximations to perform learning and inference.

The RPM joint for the SSM graphical model is

$$\tilde{p}_\theta^{\mathbf{X}}(\mathbf{x}, \mathbf{z}) = p_\eta(z_1) \prod_{t=1}^{T-1} p_\eta(z_{t+1}|z_t) \prod_{t=1}^T \frac{f_{\phi_t}(\mathbf{z}|x_t)p_0(x_t)}{F_{\phi_t}(\mathbf{z})}.$$

Inspired by the factorization of emissions over time in the SSM joint in Equation (3), we define the recognition factors as distributions only on z_t :

$$\tilde{p}_\theta^{\mathbf{X}}(\mathbf{x}, \mathbf{z}) = p_\eta(z_1) \prod_{t=1}^{T-1} p_\eta(z_{t+1}|z_t) \prod_{t=1}^T \frac{f_{\phi_t}(z_t|x_t)p_0(x_t)}{F_{\phi_t}(z_t)}, \quad (4)$$

and refer to this form as a recognition-parametrized SSM. The free energy for N time series observations $\mathbf{X} = (x_1^n, \dots, x_T^n)_{n=1}^N$ is

$$\mathcal{F}(\{q^n\}_{n=1}^N, \theta) = \sum_{n=1}^N \left[\sum_{t=1}^T \left(\left\langle \log \frac{f_{\phi_t}(z_t | x_t^n)}{F_{\phi_t}(z_t)} \right\rangle_{q^n(z_t)} + \log p_0(x_t^n) \right) - \text{KL}(q^n(z) || p_\eta(z)) \right]. \quad (5)$$

The explicit $\log p_0$ terms do not depend on θ or q^n and so do not affect the optimization. Therefore we omit them below. A key benefit of recognition parametrization is that model posteriors may be defined to lie within a tractable family even when the link to observations is arbitrarily nonlinear. To keep $q^n(z)$ (and $p_\eta(z)$) tractable, we focus on the GSSM prior. Inspired by Lemma 2.1, we parametrize the latent process as linear-Gaussian with no bias and a stationary distribution of $\mathcal{N}(0, I)$. The recognition factors then provide an arbitrary nonlinear link between observations and latents:

$$p(z_1) = \mathcal{N}(0, I), \quad p_\eta(z_t | z_{t-1}) = \mathcal{N}(Az_{t-1}, I - AA^\top), \quad f_{\phi_t}(z_t | x_t) = \mathcal{N}(\mu_\phi(x_t), \Sigma_\phi(x_t)).$$

By setting the transition covariance to $I - AA^\top$ we enforce that the GSSM remains in its stationary distribution at every time step. This is a modeling choice and is not necessary to our method. One limitation of the GSSM prior is that the linear dynamics it encodes (before noise) can only have a single isolated fixed point or hyperplane of fixed points, limiting expressivity of latent dynamics. The RP-GSSM can compensate for this in two ways: by having neural network-parametrized recognition, and by having favorable scaling with latent dimension (due to the efficiency of GSSM inference). Nonlinear dynamics can be approximated by higher-dimensional linear systems, as motivated by Koopman Operator Theory (Dogra and Redman, 2020). By combining nonlinear recognition with potentially higher latent dimensionality, the RP-GSSM can tractably model a wide range of systems, as shown in Section 5.

Note that $F_{\phi_t}(z_t)$ is a mixture of Gaussians (Equation (2)) and so $\langle \log F_{\phi_t}(z_t) \rangle_{q^n(z_t)}$ is intractable. Rather than resorting to sample-based Monte Carlo approximations, we resolve this term by adopting the *interior variational bound* (Walker et al., 2023). Introducing parametrized auxiliary factors $g_\omega^{tn}(z_t)$, not necessarily normalized, and applying Jensen’s inequality, we get

$$\begin{aligned} -\langle \log F_{\phi_t}(z_t) \rangle_{q^n(z_t)} &= -\left\langle \log \frac{F_{\phi_t}(z_t) g_\omega^{tn}(z_t) q^n(z_t)}{g_\omega^{tn}(z_t) q^n(z_t)} \right\rangle_{q^n(z_t)} \\ &\geq \left\langle \log \frac{g_\omega^{tn}(z_t)}{q^n(z_t)} \right\rangle_{q^n(z_t)} - \log \int F_{\phi_t}(z_t) g_\omega^{tn}(z_t) dz_t. \end{aligned} \quad (6)$$

If we choose $g_\omega^{tn}(z_t)$ to be proportional to a Gaussian, the right-hand side can be computed in closed form. This yields a lower bound to \mathcal{F} , which we call the *auxiliary free energy*, denoted $\mathcal{G}(\{q^n\}_{n=1}^N, \{g_\omega^{tn}\}_{n=1, t=1}^{N, T}, \theta)$. The auxiliary free energy can be optimized by alternating maximization of the q^n , ω , and θ . However, in practice we found it sufficient to update the g_ω^{tn} approximately, as follows. First, we note that the bound in Equation (6) is tight when $g_\omega^{tn}(z_t) \propto q^n(z_t)/F_{\phi_t}(z_t)$. Moreover, as discussed by Walker et al. (2023), $F_{\phi_t}(z_t) \rightarrow p_\eta(z_t)$ in the large-data in-model limit. Hence, to support this convergence, we assume $F_{\phi_t}(z_t) \approx p_\eta(z_t)$ and set $g_\omega^{tn}(z_t) = q^n(z_t)/p_\eta(z_t)$, dropping the ω subscript as there are no additional parameters to optimize. The auxiliary free energy thus becomes

$$\mathcal{G} \stackrel{+c}{=} \sum_{n=1}^N \left[\sum_{t=1}^T \left(\left\langle \log \frac{f_{\phi_t}(z_t | x_t^n) g_\omega^{tn}(z_t)}{q^n(z_t)} \right\rangle_{q^n(z_t)} - \log \Gamma_{\phi_t}^{tn} \right) - \text{KL}(q^n(z) || p_\eta(z)) \right],$$

where the terms $\Gamma_{\omega, \phi_t}^{tn}$ can be computed in closed form. A full derivation of \mathcal{G} and a discussion of the variational gap introduced by the interior variational bound are provided in Appendix B. Since $p(z_t | x_t) \propto p(z_t) p(x_t | z_t)$ (by Bayes’ rule), we further choose to parametrize $f_{\phi_t}(z_t | x_t) \propto p_\eta(z_t) f_\phi^\Delta(z_t | x_t)$, where the f_ϕ^Δ are learned time-invariant distributions. The auxiliary free energy can then be rewritten as

$$\mathcal{G} \stackrel{+c}{=} \sum_{n=1}^N \left[\sum_{t=1}^T \left(\langle \log f_\phi^\Delta(z_t | x_t^n) \rangle_{q^n(z_t)} - \log \tilde{\Gamma}_{\phi_t}^{tn} \right) - \text{KL}(q^n(z_t) || p_\eta(z_t)) \right].$$

The RP-GSSM is trained via standard EM on \mathcal{G} . Up to an additive constant independent of the q^n , \mathcal{G} has the same form as the free energy of a linear-Gaussian system with emission factor $p(x_t^n | z_t)$ replaced by

$f_\phi^\Delta(z_t|x_t^n)$. As we define the f_ϕ^Δ distributions on z_t to be Gaussian, $q^n(z_t)$ can be computed *exactly* via standard Kalman smoothing. Furthermore, as all terms in \mathcal{G} can be computed exactly, the M-step is achieved by gradient ascent on \mathcal{G} with respect to θ .

The RP-GSSM supports exact inference and avoids Monte Carlo approximations. These unique properties provide graceful scaling with latent dimensionality, as we show in Section 5.2.

4 Related Work

Early extensions of Kalman smoothing to nonlinear transition and emissions distributions include the Extended Kalman filter (EKF; Jazwinski, 1970), which linearizes around posterior means, and the Unscented Kalman filter (Wan and Van Der Merwe, 2000), which builds on the EKF by using a sampling-based approach that allows approximation up to third order.

One of the first successful VAE-based time series models was the Deep Kalman Filter (DKF; Krishnan et al., 2015). The DKF parametrizes the variational posterior q with a recurrent neural network (RNN) and uses reparametrization to take gradients through a sample-estimated free energy. The Kalman VAE (KVAE; Fraccaro et al., 2017) and Recurrent Kalman Network (RKN; Becker et al., 2019), on the other hand, combine *locally* linear latent dynamics with VAE-based generative networks. The KVAE utilizes the local linearity to enable Kalman smoothing-based posterior inference, whereas the RKN combines local linearity with factorized state beliefs to learn high-dimensional latent state representations efficiently.

Perhaps the generative method closest to the RP-GSSM is the structured VAE (SVAE; Johnson et al., 2016; Zhao and Linderman, 2023), which learns a recognition network that outputs conjugate potentials on latents. When paired with linear-Gaussian transitions, the potentials allow for exact inference via Kalman smoothing. However, unlike the RP-GSSM, the SVAE also learns an explicit generative model using reparametrization.

Contrastive Predictive Coding (CPC) (van den Oord et al., 2018) exploits the contrastive InfoNCE loss to identify a latent representation that maximizes internal predictability. Here, a recognition network summarizing past data in a sequence aims to discriminate future latents from the same sequence (positive) from draws taken from other sequences (negative). Recent extensions of contrastive learning provide ways to learn explicit latent dynamics by adding an auxiliary loss (You et al., 2022) or by integrating parametrized dynamics directly into the model’s similarity function (Laiz et al., 2025).

5 Experiments

We compare the RP-GSSM to various generative and contrastive approaches for learning latent time series from high-dimensional observations. We show that the RP-GSSM is able to outperform baselines at recovering accurate latent representations across all tasks, and even more so when background distractions are present in the observed data. These results point to the benefits of the tractable prior combined with nonlinear recognition that is not biased by the need to track an explicit generative model. We also train an *auxiliary* generative model on the RP-GSSM latents, which we show is able to “filter out” the distractions, which generative or contrastive approaches are unable to do. Additionally, we demonstrate the RP-GSSM’s ability to learn accurate predictive dynamics without the need for auxiliary objectives or masking procedures employed by other methods.

5.1 Baseline Methods, Hyperparameters, and Estimation

We compare results from the RP-GSSM against a variety of generative and contrastive baseline methods: SVAE, KVAE, DKF with four different parametric posterior families, and CPC. Full details are presented in Appendices C and D.

We ran a hyperparameter search for each model on each task, as detailed in Appendix C.3. We measured the accuracy of latent recovery by the linear regression R^2 between each model’s posterior means and the ground truth dynamical variables of each system—arguably the simplest possible downstream task. Results using nonlinear kernel ridge regression, which are qualitatively similar, are provided in Appendix E. We apply self-supervised masking to all baselines as described by Zhao and Linderman (2023), which was shown to improve predictive performance by encouraging dynamics learning. We found that the RP-GSSM does not need such schemes to learn the latent dynamics well.

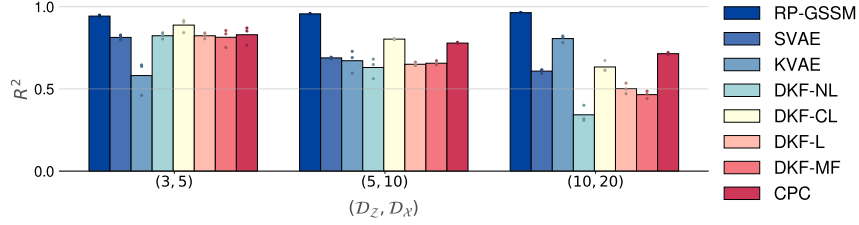


Figure 2: Linear regression R^2 score from posterior means to ground truth latent variables for the linear dynamical system, across different latent and observation dimensions. Each dot corresponds to a different seed used to generate the data.

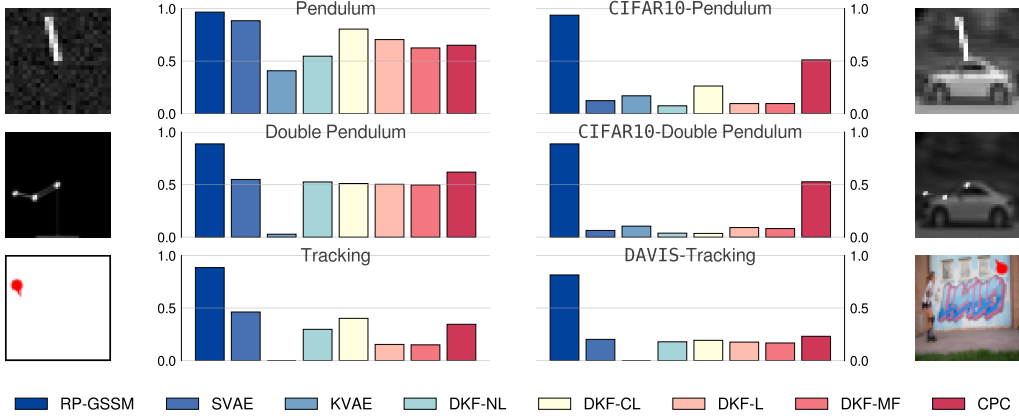


Figure 3: The mean linear regression R^2 score between inferred posterior means and true latent state variables. We find the RP-GSSM learns more informative latent representations than baselines in both the absence (left) and the presence (right) of background distractors.

5.2 Linear Dynamical System with Linear Emissions

We begin with data sampled from a linear GSSM (i.e., linear-Gaussian dynamics and emissions):

$$z_1 \sim \mathcal{N}(0, I), \quad z_t \sim \mathcal{N}(Bz_{t-1}, I - BB^\top), \quad x_t \sim \mathcal{N}(Cz_t + d, R).$$

B was a scaled rotation matrix, applying a rotation of $\pi/5$ around a randomly chosen axis, with operator norm 0.95; C and d had components sampled i.i.d from $\mathcal{N}(0, 1)$, and $R = 0.3I$. All recognition and generative networks were taken to be linear. Even in this simple setting, the RP-GSSM outperforms baselines, particularly for larger dimensionalities (Figure 2).

5.3 Pendulum and Double Pendulum

Although consideration of in-model linear dynamics is instructive, a more realistic test of the RP-GSSM is whether it can model systems with ground truth nonlinear dynamics and nonlinear observation emissions. We applied all models to datasets of noisy synthetic videos of a single pendulum (Becker et al., 2019) and real videos of a double pendulum (Asseman et al., 2018), both evolving freely under gravity from random initial conditions (see Appendix D for details). All recognition and generative networks are three-layer convolutional neural networks.

The true underlying dynamics of a pendulum are governed by angle and angular velocity, which, coupled with fixed linear acceleration due to gravity, form a nonlinear dynamical system. The dynamics of a double pendulum are higher-dimensional, nonlinear, and chaotic. The linear regression targets we use for the pendulum are sine of angle (to avoid discontinuities) and angular velocity. For the double pendulum we use the sine of the angle of the primary pendulum relative to the origin and the sine of the angle of the secondary pendulum relative to the primary pendulum. The mean linear R^2 scores to all targets are shown in the top two rows (left) of Figure 3. Despite the ground truth dynamics being

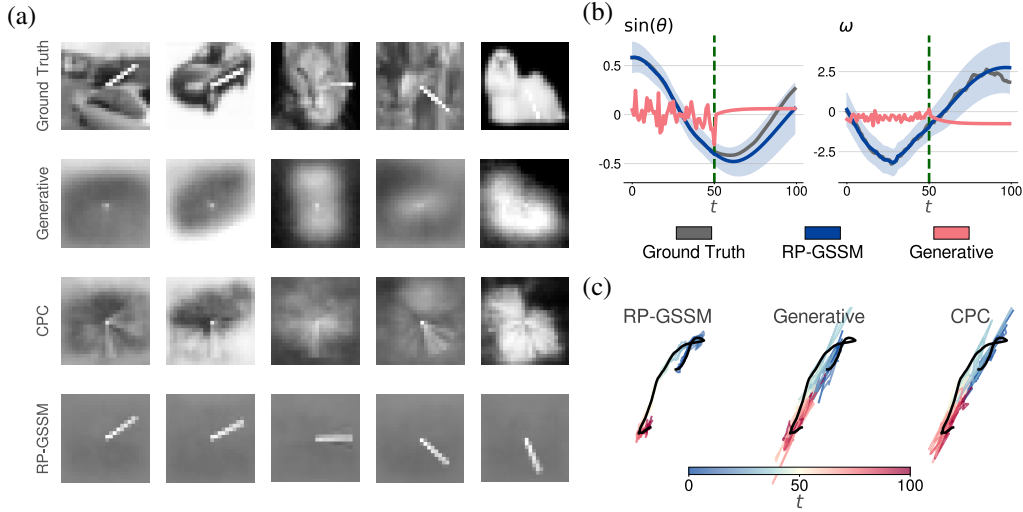


Figure 4: **(a)**: Reconstructions on CIFAR10-Pendulum for the best generative baseline and auxiliary generative models trained using the best CPC and RP-GSSM models. The RP-GSSM is the only model that allows accurate reconstruction of the pendulum arm. **(b)**: When given 50 CIFAR10-Pendulum frames as context, the RP-GSSM is able to infer the true states during the context and predict the next 50 states. The best generative baseline is unable to do either. The dashed line represents when the context ends. **(c)**: The RP-GSSM performs more accurate tracking in the DAVIS-Tracking dataset than the best generative and CPC baselines. The black line is a sample ground truth trajectory and the colored lines are inferred trajectories across five different background videos.

nonlinear, all methods perform reasonably well at decoding the targets, with the RP-GSSM being most consistent.

The ability of the RP-GSSM to perform exact inference without having to approximate a complex generative network allows for increased data efficiency. Figure 5 in Appendix E shows the results of all methods trained on only the first 64 sequences of the single-pendulum dataset. The RP-GSSM is the only model able to linearly decode angular velocity after learning on such a small dataset.

5.3.1 CIFAR10 Background Distractions

To demonstrate the performance of our model in the presence of background distractions, we apply the RP-GSSM to duplicate datasets of the pendulum and double-pendulum problems, but with randomly selected images from the CIFAR10 dataset (Krizhevsky and Hinton, 2009) in the background at each time step. We refer to these datasets as CIFAR10-Pendulum and CIFAR10-Double Pendulum.

We regress to the same targets as in the non-distractor setting. Results are shown in the top two rows (right) of Figure 3, and they clearly show that only the RP-GSSM is able to reliably decode the underlying dynamical system in the presence of distractors. While the generative baselines use model capacity on learning features of the observation backgrounds, impeding their latent state inference, the RP-GSSM ignores this and focuses on learning optimal recognition and latent dynamics models.

To illustrate the RP-GSSM’s ability to extract temporally consistent signal while ignoring distractors, we train an auxiliary generative model using the learned posteriors from the best RP-GSSM and CPC runs on CIFAR10-Pendulum. We compare reconstructions from these models with those of the best performing generative baseline in Figure 4a. Notably, only the RP-GSSM can accurately reconstruct the pendulum while ignoring irrelevant background distractions. Further details are presented in Appendix C. We also show that the RP-GSSM can be used to predict future dynamics while ignoring distractors. A sample predicted trajectory of angles and angular velocities on the CIFAR10-Pendulum dataset is shown in Figure 4b.

5.4 Object State Tracking

Finally, we apply the RP-GSSM to object state tracking from video. This task is of particular interest when it comes to real-world applications, as state tracking from visual observations is a common problem for both biological agents and in robotics.

The dataset comprises a set of synthetic video sequences simulating a rat running around a box (George et al., 2024) (see Appendix D for details). The true dynamics are governed by an Ornstein-Uhlenbeck process on the velocity vector. Position changes linearly with velocity across time steps. Although these dynamics are linear, the learned models have to deal with discontinuities in the form of barriers at the walls of the “box”, as well as having to learn from high-dimensional observations.

5.4.1 Tracking with Video Backgrounds

Similar to the CIFAR10-Pendulum and -Double Pendulum datasets above, we apply the RP-GSSM to a tracking dataset with background distractors. However, this time we apply distractions that are correlated across time, in the form of real-world videos. We stitch together randomly selected 2s video clips from the DAVIS dataset (Perazzi et al., 2016; Pont-Tuset et al., 2017) and superimpose the simulated object moving on top. We refer to this dataset as DAVIS-Tracking.

In all tracking experiments, linear regression targets were the position, velocity, and head direction (low-pass filtered velocity, red arrow in Figure 3, bottom right) of the “rat” being tracked, all of which are two-dimensional. The mean R^2 values across all targets are shown in the bottom row of Figure 3. The RP-GSSM is the only method able to consistently track the “rat”. In Figure 4c we visualize the inferred latent states for a single trajectory with 5 different background videos. The results demonstrate both the ability of the RP-GSSM to scale to high-dimensional data due to its lack of parametric generative model, as well as its robustness to changes in background distractor—something the generative and contrastive methods do not share.

6 Conclusion

Traditional probabilistic methods rely on concurrently training parametric recognition and generative models. In contrast, the RP-GSSM specifies the “generative” model implicitly in terms of the recognition process. As a result, learning is not driven by a reconstruction objective, but rather by aligning recognition and inference with the specified prior structure, i.e. by finding latent representations that capture dependencies between different observational factors. We rely on the fact that time series data naturally provides such factors in the form of observations at different time steps, and posit that “good” latent representations are those that account for the temporal structures and correlations in the observed time series. Indeed, our experiments show that this learning objective is useful for producing latent representations that more reliably filter out distractors in the observations, even if these distractors have their own internal structure (e.g. natural images and videos).

Our approach heavily relies on linear dynamical systems as the prior class for the latent time series, which makes efficient inference in the latent space possible via Kalman smoothing. Nevertheless, its applications are not limited to systems that are strictly linear. There are two sources for such nonlinearity. The first is the link between latents and observations, which can be highly nonlinear even if the true latents evolve according to linear dynamics. The second is the underlying dynamics themselves, which can be nonlinear. In both cases, the recognition network can be thought of as finding an “embedding” of the observations such that the dynamics of these embeddings can be described by a linear system. These can be of higher dimensionality than the true latents, but are still compressed relative to the full high-dimensional observations.

The general idea behind the RP-GSSM can be extended to more complicated graphical models. One future direction of work is to extend the RP-GSSM to switching dynamical systems (Dong et al., 2020). Another is to integrate control inputs into the latent dynamical system, which can be applied to simultaneous localization and mapping (Çatal et al., 2021), optimal control (Watson et al., 2019), and model-based reinforcement learning (Levine, 2018). Finally, additional data modalities such as sound, text, or reward can be incorporated into the graphical model. The resulting increase in the number of conditional independence relationships in the graph would strengthen the RP-GSSM learning signal, improving its ability to disregard irrelevant features.

References

- Asseman, A., Kornuta, T., and Ozcan, A. (2018). Learning beyond simulated physics. *Conference on Neural Information Processing Systems 2018 Spatiotemporal Workshop*.
- Baum, L. E. and Petrie, T. (1966). Statistical Inference for Probabilistic Functions of Finite State Markov Chains. *The Annals of Mathematical Statistics*, 37(6):1554 – 1563.
- Becker, P., Pandya, H., Gebhardt, G., Zhao, C., Taylor, C. J., and Neumann, G. (2019). Recurrent kalman networks: Factorized inference in high-dimensional deep feature spaces. In *International conference on machine learning*, pages 544–552. PMLR.
- Bradbury, J., Frostig, R., Hawkins, P., Johnson, M. J., Leary, C., Maclaurin, D., Necula, G., Paszke, A., VanderPlas, J., Wanderman-Milne, S., and Zhang, Q. (2018). JAX: composable transformations of Python+NumPy programs.
- Buesing, L., Macke, J. H., and Sahani, M. (2012). Learning stable, regularised latent models of neural population dynamics. *Network: Computation in Neural Systems*, 23(1-2):24–47. PMID: 22663075.
- Catal, O., Jansen, W., Verbelen, T., Dhoedt, B., and Steckel, J. (2021). Latentslam: unsupervised multi-sensor representation learning for localization and mapping. In *IEEE International Conference on Robotics and Automation, ICRA 2021, Xi'an, China, May 30 - June 5, 2021*, pages 6739–6745. IEEE.
- Chang, P., Harper-Donnelly, G., Kara, A., Li, X., Linderman, S., and Murphy, K. (2024). DYNAMAX: State space models library in jax.
- Cremer, C., Li, X., and Duvenaud, D. (2018). Inference suboptimality in variational autoencoders. In Dy, J. and Krause, A., editors, *Proceedings of the 35th International Conference on Machine Learning*, volume 80 of *Proceedings of Machine Learning Research*, pages 1078–1086. PMLR.
- Dempster, A. P., Laird, N. M., and Rubin, D. B. (1977). Maximum likelihood from incomplete data via the EM algorithm. *Journal of the Royal Statistical Society: Series B*, 39:1–38.
- Dogra, A. S. and Redman, W. (2020). Optimizing neural networks via koopman operator theory. In Larochelle, H., Ranzato, M., Hadsell, R., Balcan, M., and Lin, H., editors, *Advances in Neural Information Processing Systems*, volume 33, pages 2087–2097. Curran Associates, Inc.
- Dong, Z., Seybold, B. A., Murphy, K., and Bui, H. H. (2020). Collapsed amortized variational inference for switching nonlinear dynamical systems. In *Proceedings of the 37th International Conference on Machine Learning, ICML 2020, 13-18 July 2020, Virtual Event*, volume 119 of *Proceedings of Machine Learning Research*, pages 2638–2647. PMLR.
- Fraccaro, M., Kamronn, S., Paquet, U., and Winther, O. (2017). A disentangled recognition and nonlinear dynamics model for unsupervised learning. In Guyon, I., von Luxburg, U., Bengio, S., Wallach, H. M., Fergus, R., Vishwanathan, S. V. N., and Garnett, R., editors, *Advances in Neural Information Processing Systems 30: Annual Conference on Neural Information Processing Systems 2017, December 4-9, 2017, Long Beach, CA, USA*, pages 3601–3610.
- Friston, K., Moran, R. J., Nagai, Y., Taniguchi, T., Gomi, H., and Tenenbaum, J. (2021). World model learning and inference. *Neural Networks*, 144:573–590.
- George, T. M., Rastogi, M., de Cothi, W., Clopath, C., Stachenfeld, K., and Barry, C. (2024). Ratinabox, a toolkit for modelling locomotion and neuronal activity in continuous environments. *eLife*, 13.
- Ghahramani, Z. and Hinton, G. E. (1996). Parameter estimation for linear dynamical systems. Technical report, Department of Computer Science, University of Toronto.
- Gregor, K., Danihelka, I., Graves, A., Rezende, D., and Wierstra, D. (2015). Draw: A recurrent neural network for image generation. In Bach, F. and Blei, D., editors, *Proceedings of the 32nd International Conference on Machine Learning*, volume 37 of *Proceedings of Machine Learning Research*, pages 1462–1471, Lille, France. PMLR.
- Gu, A. and Dao, T. (2024). Mamba: Linear-time sequence modeling with selective state spaces. In *First Conference on Language Modeling*.

- Jazwinski, A. H. (1970). Stochastic processes and filtering theory. In *Stochastic Processes and Filtering Theory*, volume 64 of *Mathematics in Science and Engineering*. Elsevier.
- Johnson, M. J., Duvenaud, D. K., Wiltchko, A., Adams, R. P., and Datta, S. R. (2016). Composing graphical models with neural networks for structured representations and fast inference. In Lee, D., Sugiyama, M., Luxburg, U., Guyon, I., and Garnett, R., editors, *Advances in Neural Information Processing Systems*, volume 29. Curran Associates, Inc.
- Kalman, R. E. (1960). A new approach to linear filtering and prediction problems. *Transactions of the ASME—Journal of Basic Engineering*, 82(Series D):35–45.
- Kirchhof, M., Kasneci, E., and Oh, S. J. (2023). Probabilistic contrastive learning recovers the correct aleatoric uncertainty of ambiguous inputs. In Krause, A., Brunskill, E., Cho, K., Engelhardt, B., Sabato, S., and Scarlett, J., editors, *Proceedings of the 40th International Conference on Machine Learning*, volume 202 of *Proceedings of Machine Learning Research*, pages 17085–17104. PMLR.
- Krishnan, R. G., Shalit, U., and Sontag, D. (2015). Deep kalman filters.
- Krizhevsky, A. and Hinton, G. (2009). Learning multiple layers of features from tiny images. Technical report, University of Toronto, Toronto, Ontario.
- Laiz, R. G., Schmidt, T., and Schneider, S. (2025). Self-supervised contrastive learning performs non-linear system identification. In *The Thirteenth International Conference on Learning Representations*.
- Levine, S. (2018). Reinforcement learning and control as probabilistic inference: Tutorial and review. *CoRR*, abs/1805.00909.
- Orbán, G., Fiser, J., Aslin, R. N., and Lengyel, M. (2008). Bayesian learning of visual chunks by human observers. *Proceedings of the National Academy of Sciences*, 105(7):2745–2750.
- Perazzi, F., Pont-Tuset, J., McWilliams, B., Van Gool, L., Gross, M., and Sorkine-Hornung, A. (2016). A benchmark dataset and evaluation methodology for video object segmentation. In *Proceedings of the IEEE conference on computer vision and pattern recognition*, pages 724–732.
- Pont-Tuset, J., Perazzi, F., Caelles, S., Arbeláez, P., Sorkine-Hornung, A., and Van Gool, L. (2017). The 2017 davis challenge on video object segmentation. *arXiv:1704.00675*.
- Turner, R. E. and Sahani, M. (2011). *Two problems with variational expectation maximisation for time series models*, page 104–124. Cambridge University Press.
- van den Oord, A., Li, Y., and Vinyals, O. (2018). Representation learning with contrastive predictive coding. *ArXiv*, abs/1807.03748.
- Walker, W. I., Soulat, H., Yu, C., and Sahani, M. (2023). Unsupervised representation learning with recognition-parametrised probabilistic models. In Ruiz, F., Dy, J., and van de Meent, J.-W., editors, *Proceedings of The 26th International Conference on Artificial Intelligence and Statistics*, volume 206 of *Proceedings of Machine Learning Research*, pages 4209–4230. PMLR.
- Wan, E. and Van Der Merwe, R. (2000). The unscented kalman filter for nonlinear estimation. In *Proceedings of the IEEE 2000 Adaptive Systems for Signal Processing, Communications, and Control Symposium (Cat. No.00EX373)*, pages 153–158.
- Watson, J., Abdulsamad, H., and Peters, J. (2019). Stochastic optimal control as approximate input inference. In Kaelbling, L. P., Kragic, D., and Sugiura, K., editors, *3rd Annual Conference on Robot Learning, CoRL 2019, Osaka, Japan, October 30 - November 1, 2019, Proceedings*, volume 100 of *Proceedings of Machine Learning Research*, pages 697–716. PMLR.
- You, B., Arenz, O., Chen, Y., and Peters, J. (2022). Integrating contrastive learning with dynamic models for reinforcement learning from images. *Neurocomputing*, 476:102–114.
- Zhang, A., McAllister, R. T., Calandra, R., Gal, Y., and Levine, S. (2021). Learning invariant representations for reinforcement learning without reconstruction. In *9th International Conference on Learning Representations, ICLR 2021, Virtual Event, Austria, May 3-7, 2021*. OpenReview.net.

- Zhang, M., Vikram, S., Smith, L. M., Abbeel, P., Johnson, M. J., and Levine, S. (2019). SOLAR: deep structured representations for model-based reinforcement learning. In Chaudhuri, K. and Salakhutdinov, R., editors, *Proceedings of the 36th International Conference on Machine Learning, ICML 2019, 9-15 June 2019, Long Beach, California, USA*, volume 97 of *Proceedings of Machine Learning Research*, pages 7444–7453. PMLR.
- Zhao, Y. and Linderman, S. (2023). Revisiting structured variational autoencoders. In *International Conference on Machine Learning*, pages 42046–42057. PMLR.

A Proof of Lemma 2.1

Lemma 2.1 *Let the GSSM on observations $\mathbf{x} = (x_1 \dots, x_T)$ and latents $\mathbf{z} = (z_1, \dots, z_T)$, with parameters $\Theta = (m_1, Q_1, A, b, Q, f, g)$ be stable. Then there exists another stable GSSM with parameters $\tilde{\Theta} = (\tilde{m}_1, \tilde{Q}_1, \tilde{A}, \tilde{b}, \tilde{Q}, \tilde{f}, \tilde{g})$ such that*

$$p(\mathbf{x}|\Theta) = p(\mathbf{x}|\tilde{\Theta}),$$

the stationary distribution of the latent variables is $\mathcal{N}(0, I)$, and $\tilde{b} = 0$.

Proof. The GSSM with parameters

$$\Theta = (m_1, Q_1, A, b, Q, f, g)$$

defines a joint distribution on (z_1, \dots, z_T) and (x_1, \dots, x_T) according to

$$\begin{aligned} z_1 &\sim \mathcal{N}(m_1, Q_1), \\ z_t|z_{t-1} &\sim \mathcal{N}(Az_{t-1} + b, Q) && \text{for } t = 2 \dots T, \text{ and} \\ x_t|z_t &\sim \mathcal{N}(f(z_t), g(z_t)), && \text{for } t = 1 \dots T. \end{aligned}$$

Let G be invertible, and consider the variables $u_t := Gz_t + c$ for all t . Using the properties of Gaussian distributions under affine transformations of variables we have

$$u_1 \sim \mathcal{N}(Gm_1 + c, GQ_1G^\top)$$

and

$$u_t|z_{t-1} \sim \mathcal{N}(GAz_{t-1} + c + Gb, GQG^\top)$$

or, noting that $z_t = G^{-1}(u_t - c)$,

$$u_t|u_{t-1} \sim \mathcal{N}(GAG^{-1}u_{t-1} + (I - GAG^{-1})c + Gb, GQG^\top) \quad \text{for } t = 2 \dots T.$$

Furthermore,

$$x_t|u_t \sim \mathcal{N}(f(G^{-1}(u_t - c)), g(G^{-1}(u_t - c))),$$

or

$$x_t|u_t \sim \mathcal{N}((f \circ h)(u_t), (g \circ h)(u_t)),$$

where $h : u_t \mapsto G^{-1}(u_t - c)$.

Therefore, the variables (u_1, \dots, u_T) and emissions (x_1, \dots, x_T) are jointly distributed according to a GSSM with parameters

$$\tilde{\Theta} := (Gm_1 + c, GQ_1G^\top, GAG^{-1}, (I - GAG^{-1})c + Gb, GQG^\top, f \circ h, g \circ h). \quad (7)$$

The emission variables were left unchanged by the transformation, and so

$$p(\mathbf{x}|\Theta) = p(\mathbf{x}|\tilde{\Theta}).$$

The transition matrices on z_t and u_t , given by A and GAG^{-1} respectively, are similar and hence have the same eigenvalues. Therefore $\rho(A) = \rho(GAG^{-1})$ and the GSSM given by $\tilde{\Theta}$ for any invertible G is stable.

Next, let the stationary distribution of z_t be $\mathcal{N}(m_\infty, Q_\infty)$. The stationary distribution p_∞ satisfies

$$p_\infty(z_{t+1}) = \int p(z_{t+1}|z_t)p_\infty(z_t) dz_t,$$

which yields the *Lyapunov equation*:

$$Q_\infty = AQ_\infty A^\top + Q, \quad (8)$$

as well as an equation for the stationary mean:

$$m_\infty = Am_\infty + b. \quad (9)$$

Denote the stationary distribution of the system with parameters $\tilde{\Theta}$ by $\mathcal{N}(\tilde{m}_\infty, \tilde{Q}_\infty)$. \tilde{Q}_∞ satisfies

$$\tilde{Q}_\infty = GQ_\infty G^\top.$$

Q_∞ is symmetric positive definite and can be decomposed as $Q_\infty = USU^\top$ where U is orthogonal and S is diagonal. Setting $G := S^{-1/2}U^\top$ gives

$$\tilde{Q}_\infty = I.$$

Next, note that in Equation (9), if the bias b is 0, then $Am_\infty = m_\infty$. However, this would imply that A has an eigenvalue of 1; a contradiction. Therefore, $b = 0 \implies m_\infty = 0$.

The bias of the system defined by $\tilde{\Theta}$, given in Equation (7), is $(I - GAG^{-1})c + Gb$. Setting to 0 and solving for c ,

$$c = (GAG^{-1} - I)^{-1}Gb.$$

This equation has a unique solution for c if and only if $|GAG^{-1} - I| \neq 0$. This is the case if and only if GAG^{-1} does not have an eigenvalue equal to 1. However, as established previously, GAG^{-1} has eigenvalues equal to those of A , which cannot be 1 by assumption. Therefore, there exists a vector c such that the system defined by $\tilde{\Theta}$ has zero bias, and therefore, as argued above, also has stationary mean \tilde{m}_∞ equal to 0. This completes the proof. \square

B The RP-GSSM Loss

B.1 Variational Gaps

The RP-GSSM free energy, as defined in Equation (5), is given by

$$\mathcal{F}(\{q^n\}_{n=1}^N, \theta) = \sum_{n=1}^N \left[\sum_{t=1}^T \left(\left\langle \log \frac{f_{\phi_t}(z_t|x_t^n)}{F_{\phi_t}(z_t)} \right\rangle_{q^n(z_t)} + \log p_0(x_t^n) \right) - \text{KL}(q^n(z) || p_\eta(z)) \right]. \quad (5)$$

The free energy is a lower bound to the log-likelihood of the data under the RP-GSSM joint distribution (Equation (1)):

$$\mathcal{F}(\{q^n\}_{n=1}^N, \theta) \leq \sum_{n=1}^N \log \tilde{p}_\theta^{\mathbf{X}}(\mathbf{x}^n),$$

where $\mathbf{x}^n = (x_1^n, \dots, x_T^n)$. The difference between the data log-likelihood and the free energy is called a *variational gap* and can be written explicitly:

$$\log \tilde{p}_\theta^{\mathbf{X}}(\mathbf{x}^n) - \mathcal{F}(\{q^n\}_{n=1}^N, \theta) = \sum_{n=1}^N \text{KL}(q^n(z) || \tilde{p}_\theta^{\mathbf{X}}(z|\mathbf{x}^n)).$$

Using the interior variational bound described in Equation (6), we obtain the RP-GSSM auxiliary free energy:

$$\begin{aligned} \mathcal{G}(\{q^n\}_{n=1}^N, \{g_\omega^{tn}\}_{n=1, t=1}^{N, T}, \theta) &= \sum_{n=1}^N \left[\sum_{t=1}^T \left(\left\langle \log \frac{f_{\phi_t}(z_t|x_t^n)g_\omega^{tn}(z_t)}{q^n(z_t)} \right\rangle_{q^n(z_t)} - \log \Gamma_{\phi_t}^{tn} \right) \right. \\ &\quad \left. - \text{KL}(q^n(z) || p_\eta(z)) \right] - TN \log N \\ &\leq \mathcal{F}(\{q^n\}_{n=1}^N, \theta), \end{aligned} \quad (10)$$

where the terms $\log \Gamma_{\phi_t}^{tn}$ are given explicitly in Equation (6):

$$\begin{aligned} \Gamma_{\phi_t}^{tn} &= \int F_{\phi_t}(z_t)g_\omega^{tn}(z_t) dz_t \\ &= \frac{1}{N} \sum_{n'=1}^N \int f_{\phi_t}(z_t|x_t^{n'})g_\omega^{tn}(z_t) dz_t. \end{aligned} \quad (11)$$

The gap induced by using Jensen's inequality in Equation (6) can also be written explicitly:

$$\begin{aligned} \log \tilde{p}_\theta^X(\mathbf{x}^n) - \mathcal{G}\left(\{q^n\}_{n=1}^N, \{g_\omega^{tn}\}_{n=1, t=1}^{N, T}, \theta\right) \\ = \sum_{n=1}^N \text{KL}(q^n(z) \parallel \tilde{p}_\theta^X(z|\mathbf{x}^n)) - \sum_{n=1}^N \sum_{t=1}^T \text{KL}\left(q^n(z_t) \parallel \frac{F_{\phi_t}(z_t)g_\omega^{tn}(z_t)}{\Gamma_{\phi_t}^{tn}}\right). \end{aligned}$$

The former variational gap vanishes when q^n approaches the true posterior implied by the RP-GSSM joint. The latter gap vanishes when $g_\omega^{tn}(z_t) \propto q^n(z_t)/F_{\phi_t}(z_t)$, as also implied by Jensen's inequality in Section 3.

B.2 Loss Derivation

The full RP-GSSM auxiliary free energy is provided above in Equation (10). Although in the main text we assume Gaussian distributions throughout, here we allow any exponential family with constant base measure for generality (dropping parameter subscripts for clarity):

$$\begin{aligned} f(z_t|x_t^n) &= e^{\eta(x_t^n)^\top t(z_t) - \Phi(\eta(x_t^n))} \\ q^n(z_t) &= e^{(\eta_{qt}^n)^\top t(z_t) - \Phi(\eta_{qt}^n)} \\ p(z_t) &= e^{\eta_{0t}^\top t(z_t) - \Phi(\eta_{0t})}. \end{aligned}$$

I.e., the terms above belong to the same exponential family but with different natural parameters. Let the auxiliary factors $g^{tn}(z_t)$ have the same shape and their own natural parameters $\tilde{\eta}_t^n$:

$$g^{tn}(z_t) = e^{(\tilde{\eta}_t^n)^\top t(z_t)}.$$

The auxiliary factors do not have to be normalized, so we model them without log-normalizer (Φ) terms. With this parametrization, the Γ^{tn} terms from Equation (11) become

$$\begin{aligned} \Gamma^{tn} &= \frac{1}{N} \sum_{n'=1}^N \int e^{(\eta(x_t^{n'}) + \tilde{\eta}_t^n)^\top t(z_t) - \Phi(\eta(x_t^{n'}))} dz_t \\ &= \frac{1}{N} \sum_{n'=1}^N e^{\Phi(\eta(x_t^{n'}) + \tilde{\eta}_t^n) - \Phi(\eta(x_t^{n'}))}. \end{aligned} \quad (12)$$

In Section 3 we introduced the parametrizations $g^{tn}(z_t) \propto q^n(z_t)/p(z_t)$ and $f(z_t|x_t^n) \propto p(z_t)f^\Delta(z_t|x_t^n)$. In the interior variational bound we multiply and divide by g^{tn} , so these terms can be multiplied by arbitrary constants which cancel out. The terms $f(z_t|x_t^n)$, on the other hand, are normalized to be valid probability distributions. In natural parameter space the equivalent parametrizations are

$$\begin{aligned} \tilde{\eta}_t^n &= \eta_{qt}^n - \eta_{0t} \\ \eta(x_t^n) &= \eta_{0t} + \eta^\Delta(x_t^n), \end{aligned}$$

where $\eta^\Delta(x_t^n)$ are the natural parameter corresponding to $f^\Delta(z_t|x_t^n)$ (which is a member of the same exponential family as all other distributions above). In addition to supporting the convergence $F(z_t) \rightarrow p(z_t)$ in the large-data in-model limit, this parametrization ensures that the natural parameters in Equation (12), i.e., $\eta(x_t^{n'})$ and $\eta(x_t^{n'}) + \tilde{\eta}_t^n$, are valid natural parameters for all n, n', t . In particular, when all distributions are Gaussian, the parametrization ensures that all covariance matrices are positive definite, avoiding singularities.

The normalizing constant for $f(z_t|x_t^n)$, denoted Z^{tn} , is given by

$$f(z_t|x_t^n) = \underbrace{e^{-\Phi(\eta_{0t} + \eta^\Delta(x_t^n)) + \Phi(\eta_{0t}) + \Phi(\eta^\Delta(x_t^n))}}_{1/Z^{tn}} p(z_t) f^\Delta(z_t|x_t^n).$$

Putting everything together, the interior variational bound is

$$\begin{aligned} \left\langle \log \frac{f(z_t|x_t^n)}{F(z_t)} \right\rangle_{q^n(z_t)} &\geq \left\langle \log \frac{f(z_t|x_t^n)g^{tn}(z_t)}{q^n(z_t)} \right\rangle_{q^n(z_t)} - \log \Gamma^{tn} \\ &= \langle \log f^\Delta(z_t|x_t^n) \rangle_{q^n(z_t)} - \log Z^{tn} - \log \Gamma^{tn} \\ &= \langle \log f^\Delta(z_t|x_t^n) \rangle_{q^n(z_t)} - \log \tilde{\Gamma}^{tn}, \end{aligned}$$

where

$$\log \tilde{\Gamma}^{tn} = \Phi(\eta_{0t} + \eta^\Delta(x_t^n)) - \Phi(\eta_{0t}) - \Phi(\eta^\Delta(x_t^n)) - \log N + \sum_{n'=1}^N e^{\Phi(\eta_{0t} + \eta^\Delta(x_t^{n'})) - \Phi(\eta_{0t} + \eta^\Delta(x_t^n))}.$$

This yields the final loss presented in Section 3:

$$\mathcal{G}(\{q^n\}_{n=1}^N, \theta) = \sum_{n=1}^N \left[\sum_{t=1}^T \left(\langle \log f_\phi^\Delta(z_t | x_t^n) \rangle_{q^n(z_t)} - \log \tilde{\Gamma}_{\eta, \phi}^{tn} \right) - \text{KL}(q^n(z) || p_\eta(z)) \right],$$

where $\theta = (\eta, \phi)$. The terms g_ω^{tn} are dropped from the arguments of \mathcal{G} because they are now defined in terms of θ and the q^n .

C Implementation Details

All implementation was done in jax (Bradbury et al., 2018), using the dynamax package (Chang et al., 2024) for Kalman smoothing.

C.1 Baselines

Here we provide details of the baseline models used in this work. We follow Zhao and Linderman (2023) in the implementation of the SVAE and DKF baselines, and our code for these was adapted from their code repository. These models have a linear-Gaussian prior chain over the latents and neural-network parametrized Gaussian emissions with constant diagonal covariance:

$$\begin{aligned} z_1 &\sim \mathcal{N}(m_1, Q_1) \\ z_t | z_{t-1} &\sim \mathcal{N}(Az_{t-1} + b, Q) \\ x_t | z_t &\sim \mathcal{N}(\mu_\theta(z_t), \sigma^2 I) \end{aligned}$$

The four DKF baselines differ in their variational posterior families. These are as follows:

DKF-MF:

$$q_\phi(z_{1:T}) = \prod_{t=1}^T \mathcal{N}(z_t | \mu_{\phi,t}(x_{1:T}), \Sigma_{\phi,t}(x_{1:T}))$$

where $\{\mu_{\phi,t}(x_{1:T}), \Sigma_{\phi,t}(x_{1:T})\}_{t=1}^T$ are the outputs of a bi-directional RNN.

DKF-L:

$$q_\phi(z_{1:T}) = \mathcal{N}(z_1 | \mu_{\phi,1}(x_{1:T}), \Sigma_{\phi,1}(x_{1:T})) \prod_{t=2}^T \mathcal{N}(z_t | Az_{t-1} + \mu_{\phi,t}(x_{1:T}), \Sigma_{\phi,t}(x_{1:T}))$$

where $\{\mu_{\phi,t}(x_{1:T}), \Sigma_{\phi,t}(x_{1:T})\}_{t=1}^T$ are the outputs of a bi-directional RNN.

DKF-NL:

$$\begin{aligned} q_\phi(z_{1:T}) &= \mathcal{N}(z_1 | \mu_{\phi,1}(x_{1:T}), \Sigma_{\phi,1}(x_{1:T})) \\ &\cdot \prod_{t=2}^T \mathcal{N}(z_t | g_\phi(z_{1:t-1}, u_{\phi,t}(x_{1:T})), G_{\phi,t}(z_{1:t-1}, u_{\phi,t}(x_{1:T}))) \end{aligned}$$

where g_ϕ and G_ϕ are neural networks, and $\{u_{\phi,t}(x_{1:T})\}_{t=1}^T$ are the outputs of a bi-directional RNN.

DKF-CL:

$$q_\phi(z_{1:T}) = \mathcal{N}(z_1 | \mu_{\phi,1}(x_{1:T}), \Sigma_{\phi,1}(x_{1:T})) \prod_{t=2}^T \mathcal{N}(z_t | Az_{t-1} + \mu_{\phi,t}(x_{1:T}), \Sigma_{\phi,t}(x_{1:T}))$$

where $\{\mu_{\phi,t}(x_{1:T}), \Sigma_{\phi,t}(x_{1:T})\}_{t=1}^T$ are the outputs of a convolutional neural network applied across the time dimension.

The KVAE and CPC models are parametrized in the same way as originally published in Fraccaro et al. (2017) and van den Oord et al. (2018), respectively. In particular, the CPC autoregressive model is parametrized with a forward GRU. The KVAE chain mixture weight RNN is parametrized with a forward LSTM.

C.2 Auxiliary Generative Models

The loss used to train the RP-GSSM auxiliary generative model (Figure 4a) was

$$\mathcal{L}(\psi) = \sum_{n=1}^N \sum_{t=1}^T \langle \log p_{\psi}(x_t^n | z_t) \rangle_{q^n(z_t)},$$

where ψ parametrizes the generative model:

$$p_{\psi}(x_t^n | z_t) = \mathcal{N}(x_t^n | f_{\varphi}(z_t), \sigma^2 I),$$

for $\psi = (\varphi, \sigma^2)$. The loss was estimated using samples $z_t \sim q^n(z_t)$ and optimized using the reparametrization trick to backpropagate through the samples. This is identical to the generative component of the loss used by the SVAE and the DKF.

The loss used to train the CPC auxiliary generative model was

$$\mathcal{L}(\varphi) = \sum_{n=1}^N \sum_{t=1}^T \|f_{\varphi}(c_t^n) - x_t^n\|_2^2,$$

where c_t is the *context vector* output by the recurrent network (van den Oord et al., 2018) and f_{φ} is the auxiliary generative network.

All generative networks f_{φ} are parametrized as three-layer deconvolutional neural networks followed by a sigmoid function to map to $(0, 1)$.

C.3 Hyperparameters

A learning rate of 10^{-3} was used for all runs. All runs swept over recognition covariance parametrized as either diagonal or as a Cholesky factor. The RP-GSSM was further swept over recognition covariance being data-dependent or data-independent. For all generative baseline methods, the generative covariance was taken to be constant, as is typical in the VAE literature. The generative covariance was parametrized as $\nu^2 I$, with ν swept from $\{1, 0.1, 0.001\}$.

To enforce stability of the learned latent dynamical systems we required $\rho(A) < 1$. A sufficient condition is that the largest singular value of A is less than 1. The set of matrices with singular values less than 1 is convex, simplifying constrained optimization (Buesing et al., 2012). We enforce the constraint by clipping the singular values of A to the range $(0, 1 - \epsilon)$ after each gradient step. We took $\epsilon = 10^{-3}$.

The linear and all pendulum experiments were trained for 10K iterations, whereas all tracking experiments were trained for 5K iterations.

The following latent dimensionalities were swept over:

- Single-pendulum: $\{4, 8\}$;
- Double-pendulum: $\{8, 16\}$;
- Tracking: $\{8, 16, 32\}$.

For the linear experiments, the latent dimension of all methods was set equal to the problem’s true latent dimension.

Table 1 shows the optimal parameters for the RP-GSSM in different experiments.

C.4 Compute Resources

All experiments except for those on the Tracking and DAVIS-Tracking tasks were run on a single RTX5000 GPU. Tracking experiments were run on a single RTX4090 GPU.

D Experimental Details

Each dataset consists of data sequences of $T = 100$ time steps. The number of sequences N in each dataset is as follows:

Table 1: Optimal hyperparameters for all RP-GSSM experiments from Section 5. $\mathcal{D}_{\mathcal{Z}}$ = RP-GSSM latent dimensionality; CRC = constant recognition covariance; DRC = diagonal recognition covariance; LR = learning rate.

Dataset	$\mathcal{D}_{\mathcal{Z}}$	CRC	DRC	LR	BS	Train Iters.	Optim.
Linear	–	Yes	Yes	0.001	32	10K	Adam
Pendulum	8	Yes	No	0.001	32	10K	Adam
CIFAR10-Pendulum	8	Yes	No	0.001	32	10K	Adam
Double-Pendulum	8	No	No	0.001	32	10K	Adam
CIFAR10-Double-Pendulum	16	Yes	No	0.001	32	10K	Adam
Tracking	16	Yes	No	0.001	32	5K	Adam
DAVIS-Tracking	32	Yes	No	0.001	32	5K	Adam

- **Linear:** $N = 200$;
- **Pendulum:** $N = 500$;
- **Double Pendulum:** $N = 376$;
- **Tracking:** $N = 500$.

The **Pendulum** dataset consists of sequences of 24×24 pixel frames sampled at 0.01s intervals. Pixel intensities are normalized to $(0, 1)$ and uncorrelated pixel-level zero-mean Gaussian noise with standard deviation 0.05 is applied to all frames. The **Double Pendulum** observations are 50×50 pixel frames of a real-life double pendulum system, sampled at 0.0075s intervals. Frames are single-channel grayscale for both tasks.

For the **Tracking** dataset, the observation frames are 64×64 pixels with three color channels. Each 100 frame-long sequence is equivalent to approximately 5s of real time. The “head”-direction (represented by an arrow in the observations) is computed using a low-pass filter on the velocity vector.

E Further Results

E.1 Figure 5

The RP-GSSM is the only method tested that is able to infer angular velocity when trained on only 64 data sequences.

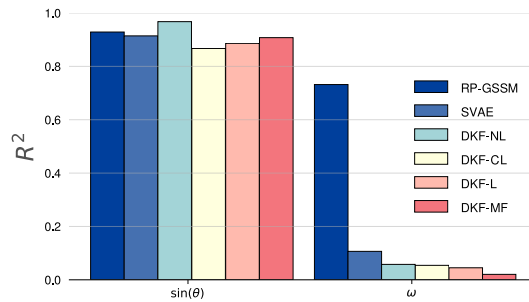


Figure 5: Linear regression R^2 scores to sine of pendulum angle, $\sin \theta$, and angular velocity, ω , of all methods trained on the first 64 sequences of the single-pendulum dataset.

E.2 Additional Regression Results

Figure 6 is identical to Figure 3, but using kernel ridge regression instead of linear regression. Regression was performed with an RBF kernel and with a fixed regularization constant across all models and tasks.

Figures 7 and 8 show R^2 scores from linear and kernel ridge regression, respectively, to all target variables. The target variables are as follows:

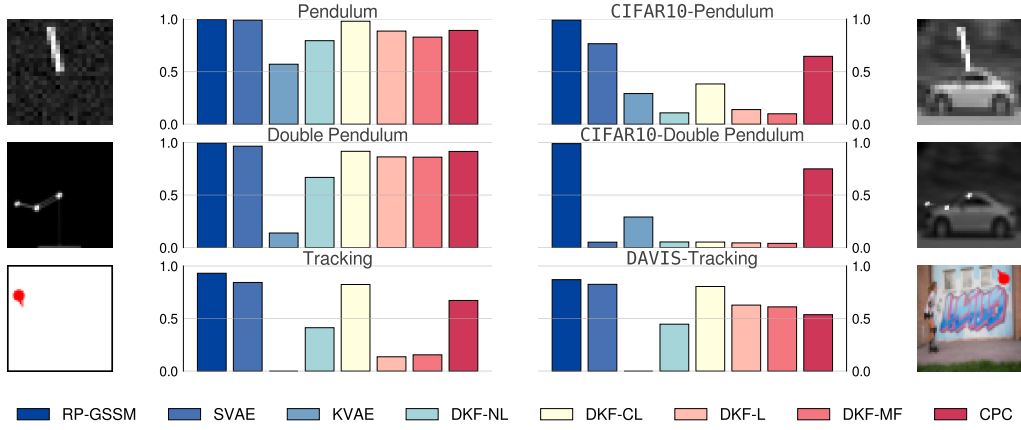


Figure 6: Mean kernel ridge regression R^2 scores.

- **Top two rows:** sine of angle, $\sin \theta$, and angular velocity, ω ;
- **Middle two rows:** sine of primary angle with respect to the origin, $\sin \theta_1$, and sine of secondary angle with respect to the primary angle, $\sin \theta_2$;
- **Bottom two rows:** rat position, x , rat velocity, v , and rat head direction, x_{head} . These have dimensionality 2, 2, and 1, respectively.

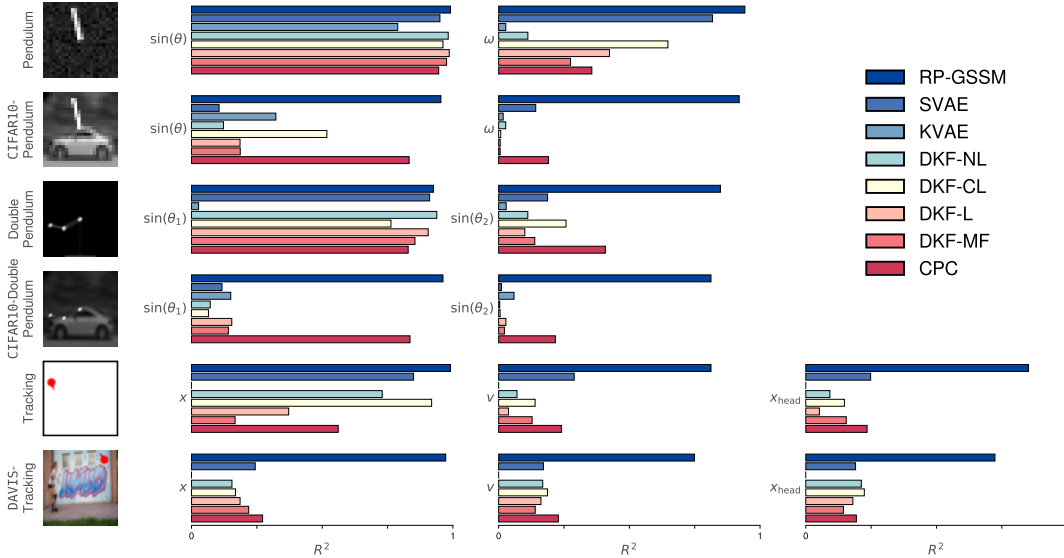


Figure 7: Linear regression R^2 scores to all target variables.

E.3 Computational Complexity and Runtimes

Figure 9 shows the mean time it takes for each model to complete one iteration, averaged over all runs in the sweeps, for the three linear tasks. The RP-GSSM has the fastest iterations. However, these times are implementation-dependent and may not necessarily be representative of true computational complexity. For completeness, we normalize each model’s times relative to its mean time on the smallest linear task. Normalized mean times are shown in Figure 10; the RP-GSSM times scale with latent and observation dimensionalities at a similar rate to the baselines models.

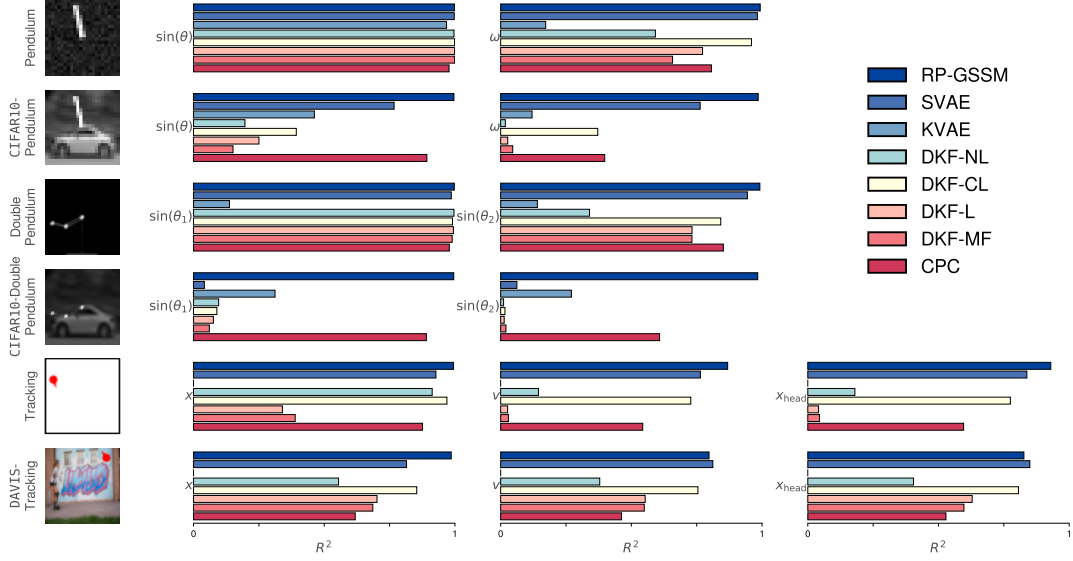


Figure 8: Kernel ridge regression R^2 scores to all target variables.

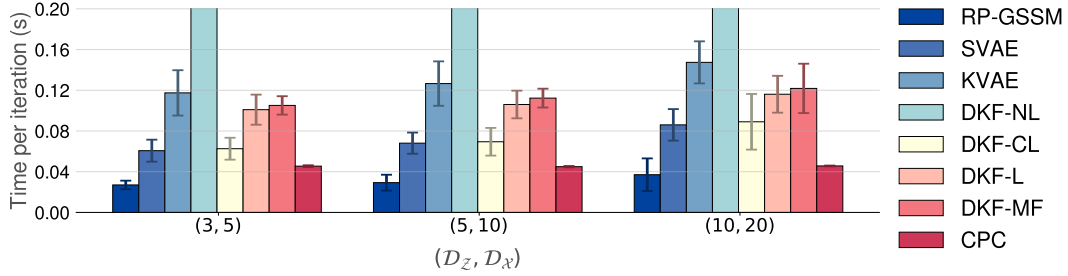


Figure 9: Average times per iteration across the full sweeps for the linear tasks. Error bars indicate standard deviation. The times for DKF-NL (approximately 0.3s) are significantly higher than for other models, so they are cropped for visual clarity.

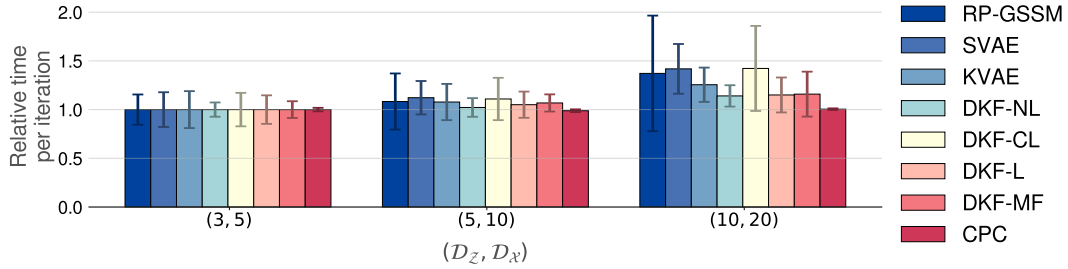


Figure 10: Average times per iteration, normalized relative to the mean time per iteration for the smallest linear task, across the full sweeps for the linear tasks. Error bars indicate standard deviation.

F Licenses

We release the RP-GSSM model and code under the CC BY-NC 4.0 license.

The assets used in this work have the following licenses:

- The CIFAR10 dataset: MIT license;
- The DAVIS dataset: BSD license;
- The code for the SVAE and DKF models (Zhao and Linderman, 2023): MIT license;

- The KVAE model: unknown license;
- The CPC model: unknown license.